Real-Time Activity Recognition With Instantaneous Characteristic Features of Thigh Kinematics

Shihao Cheng, *Member, IEEE*, Edgar Bolívar-Nieto, *Member, IEEE*, and Robert D. Gregg, *Senior Member, IEEE*

***Abstract*— Current supervised learning or deep learning-based activity recognition classifiers can achieve high accuracy in recognizing locomotion activities. Most available techniques use a high-dimensional space of features, e.g., combinations of EMG, kinematics and kinetics, and transformations over those signals. The associated classification rules are therefore complex; the machine tries to understand the human, but the human does not understand the machine. This paper presents an activity recognition system that uses signals from a thigh-mounted IMU and a force sensitive resistor to classify transitions between sitting, walking, stair ascending, and stair descending. The system uses the thigh's orientation and velocity with foot contact information at specific moments within a given activity as the features to classify transitions to other activities. We call these Instantaneous Characteristic Features (ICFs). Because these ICFs are biomechanically intuitive, they are easy for the user to understand and thus control the activity transitions of wearable robots. We assessed our classification algorithm offline using an existing dataset with 10 able-bodied subjects and online with another 10 able-bodied subjects wearing a real-time system. The offline study analyzed the effect of subject-dependency and ramp inclinations. The real-time classification accuracy was evaluated before and after training the subjects on the ICFs. The real-time system achieved overall pre-subject-training and post-subject-training error rates of 0.59% ± 0.24% and 0.56% ± 0.20%, respectively. We also evaluated the feasibility of our ICFs for amputee ambulation by analyzing a public dataset with the open-source bionic leg. The simplicity of these classification rules demonstrates a new paradigm for activity recognition where the human can understand the machine and vice-versa.**

***Index Terms*— Activity recognition, classification algorithm, wearable sensors, prosthetics, machine learning.**

Manuscript received May 1, 2021; revised July 16, 2021; accepted August 21, 2021. Date of publication August 24, 2021; date of current version September 13, 2021. This work was supported by the National Institute of Child Health and Human Development of the NIH under Award R01HD094772. The content is solely the responsibility of the authors and does not necessarily represent the official views of the NIH. *(Corresponding author: Robert D. Gregg.)*

This work involved human subjects or animals in its research. Approval of all ethical and experimental procedures and protocols was granted by the Institutional Review Board at the University of Michigan under Protocol No. HUM00166976 on 28 August 2020.

Shihao Cheng is with the Department of Mechanical Engineering, University of Michigan, Ann Arbor, MI 48109 USA, and also with the Robotics Institute, University of Michigan, Ann Arbor, MI 48109 USA (e-mail: chengsh@umich.edu).

Edgar Bolívar-Nieto and Robert D. Gregg are with the Division of Electrical and Computer Engineering, University of Michigan, Ann Arbor, MI 48109 USA, and also with the Robotics Institute, University of Michigan, Ann Arbor, MI 48109 USA (e-mail: ebolivar@ieee.org; rgregg@ieee.org).

This article has supplementary downloadable material available at https://doi.org/10.1109/TNSRE.2021.3107780, provided by the authors.

Digital Object Identifier 10.1109/TNSRE.2021.3107780

I. Introduction

RECOGNITION or prediction of human intent is fundamental to the control of wearable robots, such as exoskeletons and prostheses [1], [2]. Activity recognition algorithms allow wearable robots to adjust their control mode based on signals from onboard sensors or body-worn sensors [3]. While this can increase the control system's versatility, any misclassification of human intent may disturb gait stability or the user's trust in the system [4]. Researchers have developed various ways to accurately capture human intent, including using a key-fob, walking canes, audio, or video [5], [6]. Although these methods show promising accuracy to detect transitions between locomotion tasks, extra devices and commands can lead to a physical and cognitive burden on the user [7]. To enable more seamless and natural activity transitions, state-of-the-art methods utilize multiple mechanical sensors and/or electromyography (EMG) for locomotion recognition [7]–[9].

State-of-the-art methods can recognize the locomotion mode of the current step or even predict the intent of the next step with accuracy higher than 95% in real-time. A common way to achieve this goal is to use supervised learning algorithms with features based on statistical measures of gait information, collected over a fixed or adaptive time window before the next gait event (i.e., heel contact or toe-off) [10], [11]. Deep learning has been used to select features automatically from gait information, without any domain knowledge [12]. A human activity recognition algorithm can transform the time-series data into a frequency domain representation (spectrogram) using Short-Time Fourier Transform and then apply Convolutional Neural Networks or other deep learning networks to extract features and make classifications [13]–[15].

Although the features may differ, these methods commonly use a high-dimensional feature space to achieve satisfactory classification accuracy. For example, the kinematics-based classification system in [10] used up to 80 features from lower-limb sensors to predict walking direction, locomotion modes, and mode transitions. Recently, Bhakta *et al.* used a total of 140 features extracted from 2 encoders, 3 IMUs, and 1 load cell to train and validate user-independent classifiers [16].

To lower the dimension of the feature space, some researchers have tried to rank the relevance of features based on the Minimum-Redundancy Maximum-Relevancy algorithm [10], using Principal Component Analysis, or linear discriminant analysis [17]. However, these data-oriented methods still have complex models, either from the classification algorithm or the high-dimensional feature space, making it hard to explain how these systems make decisions especially when misclassifications happen. It is usually impossible for the user to learn how to avoid misclassifications in the future. This could reduce user confidence during locomotion, especially when approaching transitions to challenging activities such as stairs [18].

In contrast, heuristic rule-based classifiers are simple in terms of model complexity and feature dimension [3]. These methods utilize a set of fixed rules that indicate the transitions between different activity modes. For example, the method in [19] uses the gait phase, shank, and ankle states to classify stand, level-ground walking, stair ascent, and stair descent. Although the features are heuristic, the transition conditions between states remain complicated for users without specific biomechanics and engineering knowledge to understand. Some of the transitions also need to be triggered with extra volitional cues (e.g., hold a specific leg posture static for more than half a second during stair descent transition). In addition to the joint kinematics-based rules, terrain identification has also shown great success in activity recognition. The classifier in [20] utilizes the ground slope and ankle position estimated by the onboard sensors of the prosthetic leg to distinguish between level walk, ramps, and stairs. However, it requires the foot to fully contact the new terrain to classify, which resulted in a relatively long delay. Similarly, a heel-mounted IMU [21] can recognize those activities with 98.5% overall accuracy based on the foot trajectory over the new terrain.

To overcome these challenges, the classification system should be simple enough for users to understand and control activity transitions, rather than passively taking the classification results. To this end, the dimension of the feature space needs to be as low as possible with features carefully selected to be intuitive, distinctive for transitions between activities, and user-invariant. Most people with transfemoral amputation can control their residual hip joints. Thus, thigh-based features are suitable candidates for volitional task classification. The *phase variable* approach in [22] demonstrated this point by classifying activities with only thigh kinematic data. Phase variables are biomechanical signals that indicate the continuous progression through a gait cycle and can be derived from the phase angle inside a periodic orbit [23], e.g., thigh angle and its integral [24]. These periodic orbits also offer characteristic features to differentiate walking, stair ascent, and stair descent. A similar approach using A-ω features of the thigh angle demonstrated real-time activity classification with a 2-D feature space [25]. However, the features of these two methods also involved non-intuitive mathematical operations (e.g., coordinate transformations and Fast Fourier Transforms), which can be difficult for the user to understand and control.

This paper presents an activity recognition system that uses biomechanically-intuitive *instantaneous characteristic features* (ICFs) related to thigh orientation (θ_{th}) or velocity ($\dot{\theta}_{\text{th}}$) to give users intuitive control over their activity transitions. This approach is inspired by our thigh-based phase variable controllers for powered prosthetic legs [24], [26]–[29], where the user's hip motion directly controls the progression of prosthetic joint patterns. The ICFs are measurable from the same thigh-mounted IMU and can detect transitions between sit, walk, stair descent, and stair ascent. From the phase variable perspective, we consider standing to be a special case of walking (i.e., a fixed phase value), so we do not distinguish between these two activities in the classifier. We also consider different walking inclinations and speeds to be part of the same walking activity, which can be continuously parameterized by estimates of these parameters from the IMU and encoders on a prosthetic leg [28]. This paradigm results in a simpler (and more accurate) classification problem than many methods that differentiate ramps as discrete activities [7], [13], [16], [25]. We train and validate the main classifiers offline using supervised learning algorithms with a pre-recorded dataset of 10 able-bodied subjects performing different activities [30]. To evaluate real-time performance, we implement a self-contained, thigh-mounted system and present an outdoor study with another 10 able-bodied subjects. In addition, we evaluate the feasibility of our ICFs for amputee ambulation by analyzing a public dataset with the open-source bionic leg [31]. The main contributions of our method are summarized as follows:

- A real-time activity recognition system with a *one*-dimensional feature space based on an IMU and a Force Sensitive Resistor (FSR) to detect transitions between four activity classifications: Sit, Walk, Stair Descent, and Stair Ascent. These activity modes can be continuously parameterized by phase, speed, and incline using the same IMU in future prosthetic leg controllers [28].
- The derivation of three distinctive, thigh-based ICFs that differentiate these four activity modes with less than 5 ms delay. This offers an intuitive feature space that can be learned and directly controlled by the user to achieve greater than 99% classification accuracy.
- The first known comparison of classification accuracy before and after training subjects about the classifier, leveraging these intuitive classification rules.

The rest of this paper is organized as follows. Section II provides a detailed description of the design of the recognition system from a pre-recorded dataset [30]. Section III describes the setup and results of the offline and real-time experiments to evaluate the performance of the classifier. Section IV discusses these results including the limitations of the study. We conclude with key findings and future work in Section V.

II. System Design

This section explains how we developed the real-time classification system. We start with a couple of key assumptions to simplify the classification of different locomotion tasks for future applications on a phase-variable controlled prosthetic leg [27]. First, we assume the user will always proceed with the instrumented leg (e.g., the prosthetic side) during transitions. In this case, our method classifies the locomotor activity during the swing phase of the transitional stride. Additionally, because a single phase-variable controller

can facilitate walking at variable inclines and speeds [28], including standing still, our algorithm will classify standing and ramp walking (ascent and descent) as walking. That means our classifier only considers four distinct cases: Sit, Walk, Stair Ascent, and Stair Descent.

We next describe the derivation of three distinctive features and present a finite-state machine to manage the transitions between different activities. We then describe how we formulate the training datasets for the transition classifiers using a pre-recorded database [30] and introduce the classification algorithms used to train the classifiers. Finally, we introduce the feature detection system used for classification.

A. Feature Derivation

To enable intuitive transitions between activity modes without delay, our classification features are based on kinematics at distinct moments in gait, rather than over long time windows. We derived the ICFs from activity transitions recorded in an existing able-bodied human dataset [30]. Because transfemoral amputees have intact hips to control their residual thigh angle, we chose thigh-based ICFs. We derived three ICFs corresponding to the transitions between Walk and Sit, Walk and Stair Ascent (SA), and Walk and Stair Descent (SD) by analyzing kinematic differences between those activities (Fig. 1) at three specific moments: maximum hip flexion (MHF), heel strike (HS), and when $\theta_{\text{th}} = 10°$ with foot-ground contact (TH10). While MHF and HS were used to classify locomotion transitions, TH10 was the transition criteria for sitting (Fig. 2). Our feature selection avoided using the magnitude of time derivatives to make our algorithm more invariant to the transition speed and more intuitive for the subject.

First, to classify the transition between Walk and SA, we examined the thigh angle at MHF, $\theta_{\text{th,MHF}}$. Based on the dataset [30] depicted in Fig. 1(A), $\theta_{\text{th,MHF}}$ for Walk to SA (W-SA) transition is significantly higher than for Walk to SD (W-SD) transition or Walk. This also matches observations that people tend to raise their thighs much higher when ascending stairs than for other activities [32]. The MHF event occurs when the subject raises their thigh to the highest position during the swing phase, which is easy for them to understand and control. We denote $\theta_{\text{th,MHF}}$ as ICF-1.

Second, we defined our ICF between Walk and SD based on the difference between the thigh angle at MHF ($\theta_{\text{th,MHF}}$) and the thigh angle at HS ($\theta_{\text{th,HS}}$), because this difference is much higher for W-SD than W-SA or Walk according to Fig. 1(A). Although this feature is not as straightforward as ICF-1, it can be well-explained from the geometry of thigh motion. As shown in Fig. 1(B), $\theta_{\text{th,HS}}$ is closer to 0° for SD than for Walk and SA. Hence, by subtracting $\theta_{\text{th,MHF}}$ from $\theta_{\text{th,HS}}$, the Walk-SD transition generates a unique ICF, denoted as ICF-2.

Finally, transitions from Walk/Stand to Sit occur when θ_{th} reaches the 10° boundary with a positive velocity $\dot{\theta}_{\text{th}}$, and the opposite transition occurs with a negative $\dot{\theta}_{\text{th}}$. We chose a 10° threshold based on the intuition that prosthetic knee and ankle impedance would allow an amputee subject to initiate

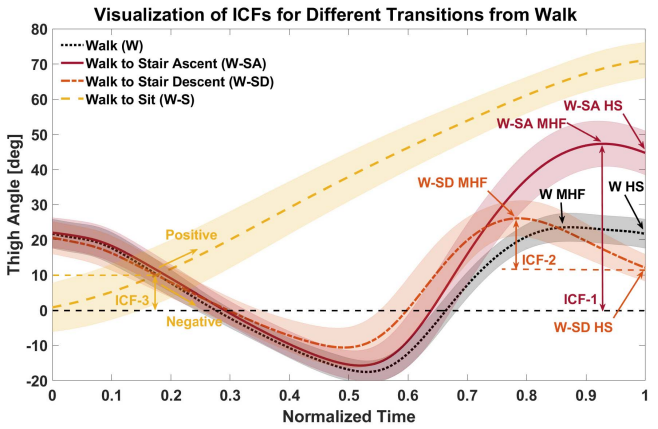

(A) Trajectories of Transitions

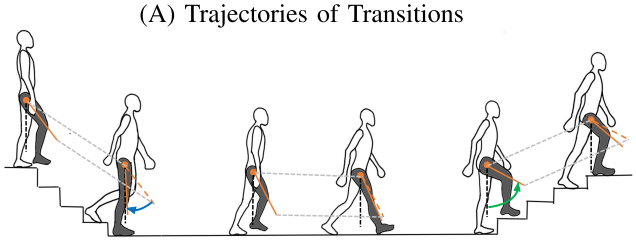

(B) MHF and HS visualization

Fig. 1. Visualization of the ICFs for different transitions. (A) Trajectories of different transitions are averaged over all trials in the dataset [30] and the shaded region around each curve shows the standard deviation. ICF-1 is θ_{th} at MHF ($\theta_{\text{th,MHF}}$), ICF-2 is the difference $\theta_{\text{th,MHF}}$ - $\theta_{th,HS}$, and ICF-3 is the sign of $\dot{\theta}_{\text{th}}$ when $\theta_{\text{th}} = 10°$. (B) The gray dashed lines represent the parallel translation of $\theta_{\text{th,MHF}}$ at MHF to visualize better the difference with $\theta_{\text{th,HS}}$ for each of the same activity. The blue arrow shows the higher ICF-2 for SD compared to Walk and SA, while the green arrow shows the significantly higher ICF-1 for SA compared to the other two. All angles are in the sagittal plane and are equal to zero when the subject is standing vertically.

the Stand-to-Sit transition until the thigh reaches about 10°. Beyond this value the joint stiffness would produce enough torque to oppose the voluntary motion of the subject, requiring the prosthesis to switch to a Stand-to-Sit controller to complete the transition. In the opposite direction, the Sit mode could utilize a phase-variable controller for Sit-to-Stand to enable the user to reach the 10° threshold to switch back to Walk [29]. This threshold could also be customized by the user. Moreover, we found that $\dot{\theta}_{\text{th}}$ is very distinctive since it is positive during the Walk to Sit (W-S) transition and negative during the opposite transition [30]. Nevertheless, it is possible for θ_{th} to reach 10° during the swing phase, so we constrained the W-S transition to only happen with foot-ground contact. Hence, the velocity $\dot{\theta}_{\text{th}}$ at TH10 was chosen as ICF-3.

B. System Logic

We used a finite state machine (FSM) with four states—Sit (S), Walk (W), Stair Ascent (SA), Stair Descent (SD)—to break the classification problem into six transition detection problems based on the current activity. Fig. 2 shows the transition diagram between states. Because Walk includes standing, we consider Walk as the bridge that connects the other three states. As shown in Fig. 2, transitions to S, SA,

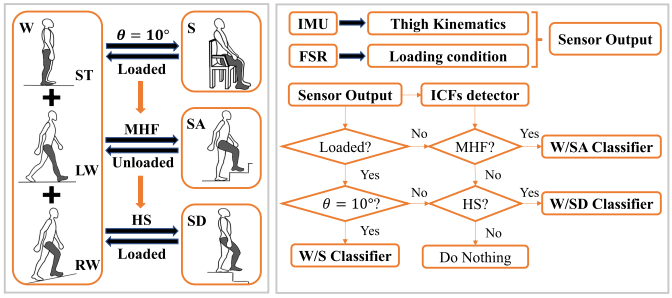

Fig. 2. Logic diagram for the activity recognition system. In the FSM, level walking (LW), stand (ST), and ramp walking (RW) are combined into the same state which can be handled by a single phase-variable controller [28]. No direct transitions are allowed between sit (S), stair ascent (SA), and stair descent (SD). In the flowchart, the ICFs detector will search for specific moments (i.e., MHF, HS) that contain different ICFs from the thigh IMU to predict the next state. Based on foot contact (FSR) and the ICF detection, different classifiers run in sequential order. Once a transition is detected, the algorithm updates the current state and breaks out of the loop.

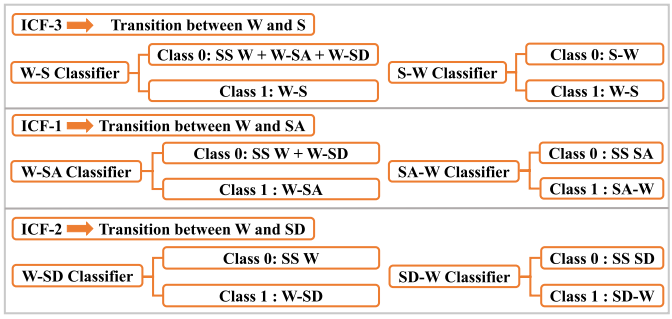

Fig. 3. Construction of the training dataset. SS represents "Steady-State", W represents "Walk", S represents "Sit", SA represents "Stair Ascent", and SD represents "Stair Descent". The "–" between each activity means "transition to". Each classifier has two classes (labeled 0 and 1). Class 1 training data corresponds to the specific transition only, whereas Class 0 training data corresponds to the steady-state task or other possible transitions from that state based on the system logic's sequential order of classifications.

and SD cannot happen until the system comes to the walk state. Thus, six classifiers (W-S, S-W, W-SA, SA-W, W-SD, and SD-W) were trained separately to reduce the complexity of classification and improve classification accuracy. In the real-time implementation, only one transition classifier (S-W, SA-W, or SD-W) will run when the current state is S, SA, or SD, respectively. If the current state is Walk, the other three transition classifiers will run in sequential order (W-S → W-SA → W-SD) once the corresponding ICFs are detected. Pseudo code is available in Supplementary Algorithm S1.

To increase the robustness of our real-time implementation in Section III-B, we updated the system logic to detect transitions from Walk to Sit by adding a checkpoint to confirm the transition at $\theta_{\text{th}} = 20°$ after classifying ICF-3 at $\theta_{\text{th}} = 10°$. This will make the classification system less susceptible to signal noise from the FSR in the real-time experiment.

C. Formulation of Training Datasets

We used the dataset [30] to train the parameters of ICF-1 and ICF-2 using supervised learning models. Fig. 3 shows how we constructed the training dataset for each classifier. Because we separately classify each transition type (Section II-B), the purpose of each classifier is to detect whether the corresponding transition happens, otherwise stay in the current activity. Hence, the training dataset for each classifier comprised two classes: Class 1 included the transitional gait only (e.g., Class 1 of the W-SA classifier only included the W-SA transition strides), and Class 0 included steady-state strides of the current classified activity and other possible transitional gaits from that activity. We determined the possible transitions based on the logic and classification sequence (W-S → W-SA → W-SD) described in Section II-B. For example, because W-S classification happens before W-SA, transitional data from W-S were not included in Class 0 for the W-SA classifier. However, since W-SD classification happens before W-SA, transitional strides of W-SD need to be included in Class 0. The same logic applies to the other classifiers.

To account for different staircases, training datasets involving SA or SD included stair inclinations varying from 20° to 35° with 5° increments. Similarly, the Walk dataset contained speeds ranging from 1.8 to 2.4 ms^{-1}. To study the effect of including ramp walking (RW) with level walking (LW), we separately trained classifiers with three different Walk datasets: (1) LW only, (2) LW + RW (±5°), (3) LW + RW (±5° and 10°). Because we manually selected the boundary of ICF-3 (sign of $\dot{\theta}_{\text{th}}$ at $\theta_{\text{th}} = 10°$), we used the datasets mainly to validate the Walk-Sit and Sit-Walk classifiers. Refer to Section III-A for details on training and validation.

D. Classification Algorithms

Due to the simplicity of the 1-D feature space based on our ICFs, we used heuristic feature-based machine learning algorithms such as k-Nearest Neighbors (KNN), Linear Discriminant Analysis (LD), Linear Support Vector Machines (SVM), Ensemble Learning (EL), Naïve Bayes (NB), and ensemble of those algorithms (Ensemble) to train the transition classifiers. Many of these algorithms, such as KNN [33], LDA [7], SVM [11], have demonstrated high classification accuracy and low computational cost in previous gait recognition studies. For each algorithm, we manually tuned the parameters based on cross-validation accuracy to optimize classification performance. The summary of the ML parameters used for training and details on the Ensemble method are available in the Supplementary Table S1. Section III-A.1 describes details on the model selection for our classification system.

E. Real-Time Detection of MHF and HS

Based on the feature derivation section, the recognition system needs to extract features at two critical moments, MHF and HS, during each gait cycle in real-time. Thus, we developed a self-contained detection algorithm for real-time implementation purposes. According to Ishmael *et al.* [32], HS can be detected using information from a thigh IMU by setting up several thresholds on the vertical acceleration, angle, and velocity. While this method can detect HS of level walking

very well, it does not generalize to different activities because the vertical acceleration is very different for SD, SA, and Walk. Because MHF is a task-invariant moment corresponding to the maximum value of θ_{th} during a cycle, a threshold-based method can be used to detect the MHF in real-time. We ran the peak search algorithm in [25] during the swing period to find local maxima of the thigh angle, and then used thresholds on thigh kinematics and detection interval to determine whether a maximum was global, corresponding to MHF.

To accurately detect HS across activities, a load cell in the foot or shank of a prosthetic leg can be used. For the able-bodied subjects in our real-time validation study, we used an FSR encapsulated in a silicone insole to emulate a load cell.

III. Human Subject Experiments

This section evaluates the activity recognition system's performance. We designed an offline experiment for initial testing and model generation based on a publicly available human dataset [30]. After achieving satisfactory offline classification accuracy, we fixed the ICFs boundaries for a real-time study with a thigh-mounted classification system in Section III-B.

A. Offline Experiment

To train and validate the recognition system, we used a dataset [30] of lower-limb kinematics and kinetics of ten able-bodied subjects (five female) walking at multiple inclines ($\pm 0°$, 5° and 10°) and speeds ($0.8\,\mathrm{ms}^{-1}$, $1\,\mathrm{ms}^{-1}$ and $1.2\,\mathrm{ms}^{-1}$), and stair ascent/descent with multiple stair inclines (20°, 25°, 30° and 35°). This dataset also includes transitions between sit and stand, walk and stairs. The data distributions across all subjects are summarized in Supplementary Table S2. Data were recorded by a Vicon motion capture system and, for applicable tasks, a Bertec instrumented treadmill. Although motion capture measurements are not equivalent to the IMU measurements used in our real-time system, motion capture is often used as ground truth for kinematics measured by IMUs [34]. Because these two methods give similar measurements of thigh angle in the sagittal plane (RMSE = 1.07° [34]), we believe it is acceptable to train the classifiers for the real-time IMU-based classification system using this offline dataset.

1) ICFs Training: Among the algorithms mentioned in Section II-D for training the ICF-based classifiers, we selected KNN, LD, and Ensemble to make a final comparison due to the low error rate in the pilot training with a few subjects and the outstanding performance in prior work [25]. The error rate was determined by the number of incorrect predictions divided by the total number of predictions in each test set. We trained all the classifiers separately using the corresponding ICFs described in Section II-A, and used 10-fold cross-validation and leave-one-subject-out cross-validation to ensure the reliability of results (i.e., not an artifact of overfitting).

We quantified performance as the system's error rate at different ramp inclinations for user-dependent and user-independent cases. Similar to previous literature [16], user-dependent cases involved 10-fold cross-validation for each subject's data. In this case, the classifiers were trained and validated for each subject separately. In the user-independent case, we used leave-one-subject-out cross-validation, which repeatedly splits the dataset into a training set of nine subjects and a testing set of one subject (for 10 total cases). To evaluate if the model, subject, and ramp inclination had a statistically significant impact on the error rate, we conducted a three-way analysis of variance (ANOVA). Then, we applied a Bonferroni post-hoc analysis to determine whether the differences between error rates under different conditions are statistically significant ($p < 0.05$). Our real-time classifiers in Section III-B use the ICFs trained with all ten subject's data.

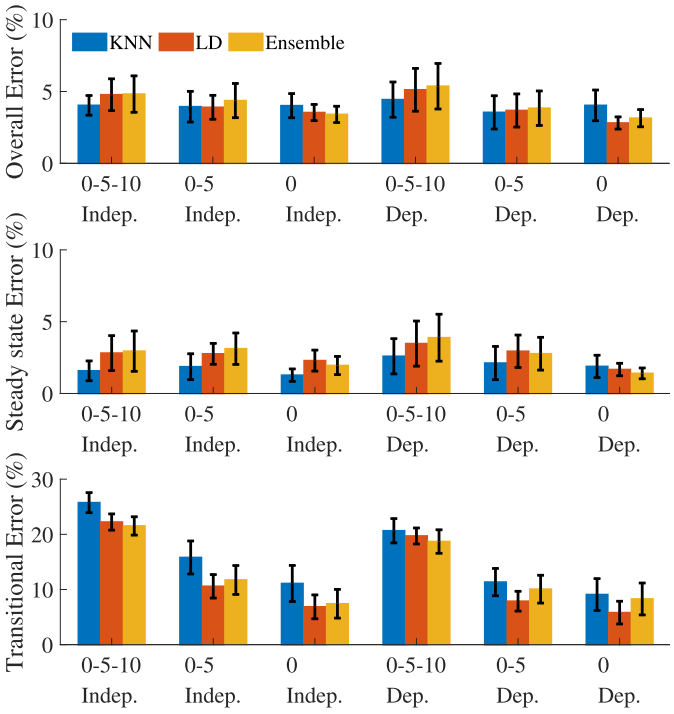

Fig. 4. Error rates for the offline experiment with data from different ramp inclinations combined with level walking for both dependent (Dep.) and independent (Indep.) cases. The label 0-5-10 means ramp inclinations at 0°, 5° and 10° were combined together, whereas 0 means only level walking was used. Error bars indicate ±1 standard error of the mean.

2) Offline Results: Fig. 4 gives the error rates for the offline cross-validations. The steady-state error corresponds to misclassifications when the current and next states are identical, whereas the transitional error accounts for non-identical cases. Overall error combines the steady-state and transitional cases. The label 0-5-10 indicates the Walk training set includes RW at 5° and 10° with LW, and 0-5 indicates RW at only 5° with LW. The ANOVAs indicate that user-dependencies, supervised learning models, and ramp inclinations are all significant factors for the transitional error rate ($p < 0.05$) but not for the overall error rate and the steady-state error rate. The interactions between each pair of these independent variables are not significant even for the transitional error rate.

Since our system focuses on transitions, the model needs to minimize transitional errors. We also want to classify RW as Walk, so we selected our final model based on the transitional error rate with the 0-5-10 training set. In the subject-dependent case, the transitional error rate of Ensemble was 18.69% ± 2.13%, which is lower than that of KNN (20.64% ± 2.20%)

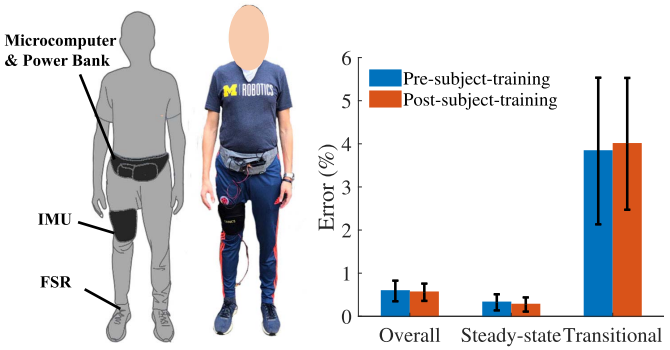

Fig. 5. Real-time experiment setup and results. Left: Participants wore a single IMU on the middle of the thigh and an FSR encapsulated in a silicon insole under the heel of the same leg. Sensors were connected to the microcomputer powered by a power bank in the waist pack. We recorded the output of the recognition system and sensor data with the microcomputer and visualized them with a host laptop that connected via hotspot. Right: Comparison of overall, steady-state, and transitional error rates of the real-time experiment before and after training the subject on the classification features. Error bars indicate ±1 standard error of the mean over relevant trials.

and LD (19.70% ± 1.45%). For the subject-independent case, Ensemble (21.52% ± 1.66%) was also better than KNN (25.75% ± 1.82%) and LD (22.23% ± 1.47%). Therefore, we picked Ensemble as the final model for the real-time experiment. For the 0-5-10 training set, Ensemble gives an overall error rate of 5.37% ± 1.59% for the subject-dependent case and 4.82% ± 1.47% for subject-independent. When ramps are removed from the set, the overall error decreases to 3.14% ± 0.60% for the subject-dependent case and 3.41% ± 0.57% for subject-independent. The ICFs boundaries are available in Supplementary Table S3.

B. Real-Time Experiment

We also performed an outdoor experiment with ten able-bodied subjects (five female; age: 26 ± 7 years, mass: 64.79 ± 21.41 kg, height: 1.72 ± 0.13 m) to evaluate the performance of a real-time implementation of the Ensemble model generated in Section III-A. The study protocol was approved on 08/28/2020 by the Institutional Review Board at the University of Michigan under protocol number HUM00166976. Written informed consent was given by each participant before the experiments.

1) Experiment Setup: The setup of the real-time classification system is shown in Fig. 5 (left). We mounted the IMU (3DM-GX5-25 AHRS, LORD MicroStrain, USA) on the middle of the thigh with a silicone IMU protector sewed on a compression sleeve to minimize motion artifacts during the experiment. The IMU has a triaxial accelerometer, gyroscope, and magnetometer and outputs signals from its dual on-board data-fusion processor running an auto-adaptive Extended Kalman Filter (EKF) in real-time. The output signals include the 3-D orientation angles, angular velocities, and linear accelerations. The IMU's built-in filter handles the common drift in IMU signals with a rated angular position error of 0.25 deg RMS in roll estimation [35].

Fig. 6. Outdoor experiment location. Left: top view of the route map of one trial, where a bench is located at the start point for sit to walk and walk to sit transitions. Right: front view of the curved ramp and three sets of stairs.

Additionally, a silicone insole with an encapsulated FSR (FSR 400, Interlink Electronics, USA) was placed inside the subject's shoe on the same leg as the IMU. A speaker provided audio feedback whenever HS was detected. An embedded system (Raspberry Pi 4, Raspberry Pi Foundation, UK) interfaced these components and ran the classifier algorithm in real-time, recording its decisions and associated classification latency. To synchronize data between sensors at 125 Hz, the embedded system sampled the FSR every time a packet was received from the IMU, resulting in a maximum delay of 8 ms based on the sample rates of both sensors. We video recorded all trials with a high-quality phone camera (iPhone X) on a stabilizing wand to later mark the transition times and generate truth tables for the locomotion activities.

At the start of each experiment, we calibrated the offset of the IMU to report zero degrees for the thigh angle in the sagittal plane when standing still. Before each trial, we performed a routine check on the sensor location and signals to ensure the precision of measurements and re-calibrated when there was an offset in the thigh angle as the subject stood still. For each trial, the subjects performed continuous transitions between Sit (S), Walk (W), Stair Ascent (SA), and Stair Descent (SD) at the outdoor location shown in Fig. 6. The transitions between S and W took place on a bench close to the starting point. Walk consisted of level walking (LW), ramp ascending (RA), ramp descending (RD), and standing (ST). The curved ramp in Fig. 6 had an average inclination of 4.8° ± 3.2° and thus evaluated the robustness of the classifiers to both changing inclines and curvature. The transitions between W and SA or SD occurred at three sets of stairs in Fig. 6, each having an inclination of 21.5°. Quarter-turn (QT) and U-turn (UT) steps were labeled as W in the construction of our truth table due to the similar kinematics profile with level walking reported by Camargo *et al.* [36]. Each subject performed a total of 10 trials: five before and five after training (discussed next). The circuit of each trial was as follows: 3 × (W→S→W) → QT → 3 × (W→SD→W) → UT → RA → W → UT → W → RD → W → UT → 3 × (W→SA→W). Subjects were asked to walk continuously at their self-selected pace. A supplemental video of the experiment is available for download.

2) Synchronization and Labelling: At the beginning of each trial, the speaker connected to the embedded system played a short beep sound to indicate the start of the data acquisition.

We captured this beep sound in the video recording to synchronize the classification outcomes and the truth table obtained from the video. Specifically, we analyzed the video using a professional video editor (Adobe Premiere Pro 2020, Adobe Inc., USA) and located the beep sound by searching through all video frames based on the audio track. We cut the video before the first frame with a beep sound so that the video start time could be synchronized with less than 34 ms delay, as the video was recorded at 30 frames per second. After that, we marked all the transition timings manually in the video editor to generate the labels for the truth table. The transition timings between activities (e.g., walk to stair ascent) were marked at toe-off of the transitional gaits, while the transition timing between sit and stand were marked at the beginning of thigh motion change. In the truth table, we set the activity label for each step to be the same as the previous step unless we manually marked a transitional step.

3) Subject Training: Thanks to the simple feature space of the thigh kinematics, it is possible to train the subjects on the boundaries and classification rules so they have more control over transitions (improving the classification accuracy). Hence, after each subject completed the first five trials, we trained them about the classification rules during a 10-minute break. We explained the three ICFs using a PowerPoint presentation and a demo script that allowed them to "feel" the boundary of each transition based on the audio feedback once they hit the transition boundary. For example, the subjects could intentionally raise their thigh higher than usual to ensure the intent of transition from Walk to Stair Ascent was captured by the system. For the Walk to Stair Descent transition, the subject could make their thigh more vertical at heel strike so that the difference between $\theta_{\text{th,MHF}}$ and $\theta_{\text{th,HS}}$ exceeded the boundary to trigger that transition. Because the ICF for the Walk to Sit transition is very distinctive and the process is natural for the subject, no further instructions were given. For transitions back to Walk, they were trained to do the opposite of the transition out of walk (e.g., lower their thigh for transitions from Stair Ascent to Walk). After training, the subject completed another five trials. Pre- and post-training error rates were calculated from their respective trials.

4) Real-Time Results: The overall classification accuracy (over all trials and subjects) before and after training was 99.41% and 99.44%, respectively. Fig. 7 shows that the accuracy for SA and SD improved from 99.5% to 100% and 97.3% to 98.7%, respectively, whereas the Walk accuracy decreased from 99.6% to 99.5% after training. Sit was predicted perfectly before and after training. Fig. 5 (right) compares the error rate before and after training in terms of the overall, steady-state, and transitional error rates. Table S4 in the supplementary material summarizes the performance of individual subjects.

A one-way ANOVA found no significant difference between the pre- and post-training steady-state error rates (0.32% ± 0.19% and 0.27% ± 0.16%, respectively). Another one-way ANOVA found no significant difference between the pre- and post-training transitional error rates (3.83% ± 0.24% and 4% ± 1.53%, respectively). Because the Walk mode includes LW, RA, RD, ST, QT, and UT during these trials, we examined the errors associated with each of these sub-activities.

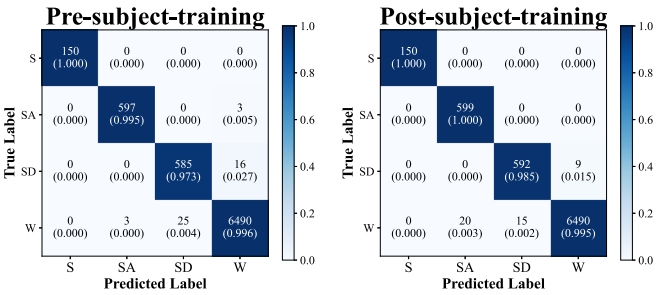

Fig. 7. Confusion matrices for Sit (S), Stair Ascent (SA), Stair Descent (SD), and Walk (W) before and after subject training on classification features in the real-time experiment. For each matrix, the y-axis represents the class from the manually labeled truth-table, while the x-axis represents the predicted class. The walking class includes ramps and turns from the outdoor trial in Fig. 6.

The pre-training trials had 28 total misclassifications; 61% (17) from LW, 32% (9) from UT, and 7% (2) from RD. The post-training trials had 35 misclassifications; 55% (19) from LW, 25% (9) from UT, 14% (5) from RD, and 6% (2) from RA.

We measured real-time performance with two metrics: classification latency and time-to-detect transition. Latency is the processing time of the classification system after reaching the corresponding landmarks to extract ICFs. Time-to-detect transition refers to the period of time between the start of a transition labeled during video processing and the moment the transition is detected. In our experiments, the latency was 3.30 ± 1.15 ms for transitions between W and SA, 0.325 ± 0.21 ms for transitions between W and SD, and 0.06 ± 0.04 ms for transitions between W and Sit. The time-to-detect transition was 497 ± 156 ms for transitions between W and SA, 677 ± 176 ms for transitions between W and SD, 375 ± 240 ms for W to Sit transitions, and 718 ± 138 ms for Sit to W transitions.

IV. Discussion

A. Offline Experiment

1) Effect of Inclinations: The ANOVA indicated that ramp inclinations significantly influence the transitional error rate. The misclassifications mostly come from ramp ascent which increases the MHF angle, especially at high inclinations. This problem was not present in the real-time experiments, possibly due to the lower ramp inclination and measuring thigh angle with an IMU rather than motion capture. We believe that with proper sensor configuration and subject training, the ICF-1 boundary for stair ascent transition can be increased to the point that it cannot be reached during ramp ascent.

2) Effect of Models: The ANOVA found no significant differences between the error rates of different supervised learning models. Because of the simple 1-D feature space with very distinctive ICFs, the boundaries between different transitions are clear and easy to separate for the traditional models we tested. Hence, the system relies less on the model selection, making it easier to understand for users without any background knowledge in the field.

3) Effect of User-Dependency: We found that subject dependency significantly affects the system during transitions, i.e., the error rate for the Indep. case is significantly higher than that of the Dep. case ($p < 0.05$). This means the classification

system could detect transitions more accurately if trained with subject-specific data. However, the steady-state error rates of the Dep. case were not significantly different than the Indep. case ($p > 0.05$), which illustrates a degree of subject-independence for the presented classification system.

B. Real-Time Experiment

1) Effect of Subject Training: We found no significant differences in error rates before and after training primarily because there was little room for improvement with a pre-subject-training accuracy of 99.41%. We observed that the false positive rate of Stair Ascent increased slightly after training (Fig. 7) because Subjects #6 and #8 (Supplementary Table S4) raised their thigh much higher than usual during the transitional step from stair ascent to walk (possibly thinking they were still ascending stairs). Although training did not influence most subjects during steady-state walking, Subjects #2 and #3 appeared to overthink the classification rules resulting in some misclassifications in 'Walk'. Additionally, Subjects #4 and #9 had more misclassifications in Stair Descent after training. Those misclassifications happened in the first three trials of the post-training experiments, which suggests that they had not adapted to the classification rules within the 10-minute training time. Based on these observations, we hypothesize that amputee subjects may perform better after longer acclimation post-training to help them control their prosthesis.

The training process demonstrated the strength of the presented system in terms of debugging misclassifications. Researchers and subjects could immediately understand why a misclassification occurred by checking the ICFs for each step and determine the best way to correct the transitions. To our knowledge, this distinguishes our methods from state-of-the-art methods and could be an essential step in bringing activity recognition techniques into clinical use on wearable robots.

2) Effect of IMU Locations: During the real-time study, we observed different subject preferences on where and how tightly the IMU strap was mounted on the thigh, which may have caused slight variations in the signals. In theory, the Kalman filter can account for different magnitudes of linear acceleration caused by different IMU locations, so that the impact on the Euler angle outputs would be minimal. Additionally, we performed a routine check and calibration of the IMU before each trial (Section III-B.1) to ensure the validity of the thigh angle measurements. In future applications to prosthetic leg control, we will mount the IMU on a fixed location above the knee hinge [27], which will eliminate the effect of IMU location in clinical use.

3) Time Delay in Recognition: According to the classification latency reported in Section III-B.4, the delay is negligible once the corresponding landmarks to extract ICFs have been reached (i.e., TH10, MHF, and HS). Therefore, the presented system can guarantee that the transitions will be made *no later* than HS, which fits well within the safe zone of smooth transitions found by Zhang *et al.* [37]. Specifically, detection of Sit-Walk (Stand) transition occurs when $\theta_{\text{th}} = 10°$ during ground contact, detection of Stair Ascent-Walk transition is around mid-swing phase, and transition of Stair Descent-Walk is detected no later than HS of the transitional step.

Note that our algorithm assumes the user proceeds with the instrumented leg (e.g., prosthesis) during transitions. If the user happens to proceed with the contralateral leg, the instrumented side will not reach the swing phase until the contralateral leg is on the new terrain, which will cause a one-step delay for activity recognition. To accommodate more transition conditions, the presented system can possibly be extended with additional ICFs when the contralateral leg leads the transition. Possible examples include the thigh angle at maximum hip extension or the ground reaction force at specific gait events, which would also be fairly intuitive.

4) Comparison With Offline Experiment: Our real-time experiment had lower steady-state and transitional error rates compared to the offline experiment, even before subject training. This is opposite to the intuition that real-time performance should be worse due to measurement noise, but can be explained in a couple ways. First, the ramp inclination angles in the real-time experiment ($4.8° \pm 3.2°$) were lower than the highest angle in the offline dataset (10°). From Fig. 4 it is obvious that the 10° incline caused higher error rates because the thigh kinematics during 10° ramp ascent are close to that of stair ascent [30]. However, according to the 2010 ADA Standards for Accessible Design [38], the maximum ramp slope is 4.76°. Hence, the presented system should work well for ADA-regulated environments. Second, ramp walking data for the offline experiment was recorded on a treadmill whereas the real-time experiment was done overground. We found that the average thigh angle during ramp ascent was smaller in the real-time experiment than in the offline experiment (with the same inclination angle), giving a much lower false-positive rate for stair ascent during the real-time experiment. One possible reason is that the belt of the treadmill drags the stance leg to a lower position compared to the overground ramp ascent, which impacts the subsequent swing phase.

It is also important to note that thigh motion during stair climbing depends on the stair inclination [30]. The stair inclination for the real-time experiment (21.5°) was very close to the *lowest* inclination in the offline dataset (20°), and the ICFs tend to be more distinctive for steeper stair inclinations [30]. This means that the error rate could be lower if the real-time system was tested on steeper stairs. The ADA-recommended angle of ascent for stairs is 20° to 32.5° [38], so we believe the presented system will perform well in daily clinical use.

C. Applicability to Amputee Subjects

We evaluated the feasibility of our classification algorithm for amputee subjects by analyzing a public dataset with the open-source bionic leg [31]. This dataset contains the averaged kinematics and kinetics data for three transfemoral amputees (two male and one female; age: 51 ± 18.5 years, time post-amputation: 25 ± 21.3 years, mass: 70.3 ± 13.8 kg, height: 1.72 ± 0.06 m) ambulating continuously between level-ground walking, ramp ascent/descent, and stair ascent/descent with the open-source bionic leg. Impedance control was used as the mid-level controller and the parameters were carefully tuned by the research team for all activities. The transitions were controlled by a microcontroller and data was captured by

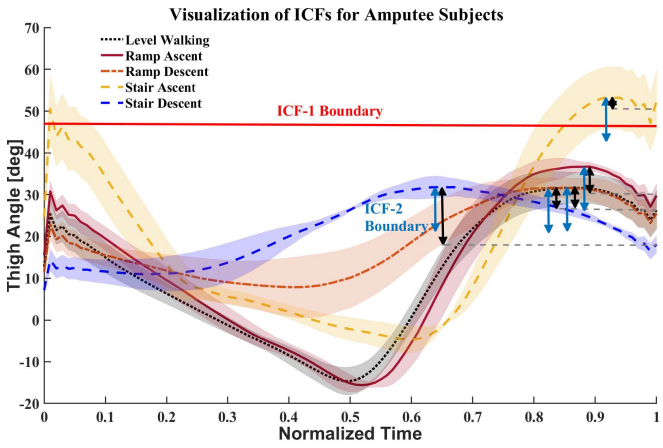

Fig. 8. Inter-subject means and standard deviations of thigh kinematics (averaged over steady-state and transition strides) for three amputee subjects using the open source leg [31]. The solid red line indicates the boundary of ICF-1 to distinguish stair ascent transition. Blue double arrows demonstrate the ICF-2 boundary with respect to the MHF of each activity to classify stair descent transition. Black double arrows represent the actual difference of thigh angle at MHF and HS as a comparison to the blue double arrows. The ICF-2 boundary will not be reached if the blue double arrow is longer than the black one (i.e., correctly ignoring transitions except the intended one: stair descent).

onboard sensors. Participants were asked to walk through the circuit 15-20 times and the data were averaged across all the steady-state and transition strides for each subject [31]. The thigh angle was estimated by a complementary filter using the gyroscope and accelerometer readings from an IMU on the shank rotated through the knee angle.

Fig. 8 shows our trained ICFs boundaries over the averaged thigh trajectories with standard deviations of those amputee subjects. The trained thresholds of ICF-1 and ICF-2 were correctly reached by only stair ascent and stair descent, respectively. Therefore, the presented ICF-based classification system can clearly separate these two activities from 'Walk' (level walking, ramp ascent, and ramp descent). Notice that this analysis was done on the reported averaged thigh trajectories over all strides, whereas Fig. 1(A) in Section II-A used only the transitional strides. Nevertheless, ICF-1 and ICF-2 are more distinctive during transitional strides than steady-state strides according to the dataset [30]. The mean stair ascent ICF-1 and stair descent ICF-2 are respectively 4.13% and 9.33% higher for transitional strides than steady-state strides, while the means of those ICFs for other activities remain similar between steady-state and transition strides. Hence, if the ICFs-based classification system can classify steady-state strides well, the performance during transitional strides would be even better. This indicates that the ICF boundaries trained with able-bodied subjects' data in this paper could also be applied to amputee subjects wearing a prosthetic leg.

D. Comparison With State-of-the-Art Methods

A direct comparison with state-of-the-art methods is challenging due to the differences in the training dataset, activity categories, sensors, and evaluation methods (e.g., offline vs. real-time). Hence, the purpose of Table I is to summarize

TABLE I
COMPARISON BETWEEN PRESENTED AND STATE-OF-ART METHODS

Method	Classified Activity	Feature Dimension*	Error Rate (%)	Instrumented Leg**
ICF	Walk#, Stairs, Sit	1	0.57	Unilateral
SVM [10]	Level Walk, Stairs, Ramps	< 80	SS: 0.2, TS: 0.4	Bilateral
CNN-Image [13]	Level Walk, Ramps, Stairs	332	1.1	Bilateral
CNN-IMUs [15]	Level Walk, Stairs, Ramps	18	AB: 5.85, AP:10.77	Healthy
XGBoost [16]	Level Walk, Stairs, Ramps	140	SS:10.12, TS:15.78	Prosthesis
GMM [17]	Level Walk, Stand, Sit	14	0	Prosthesis
Terrain Geometry [20]	Level Walk, Stairs, Ramps	2	2.8	Prosthesis
Foot-IMU [21]	Level Walk, Stairs, Ramps	2	1.5	Prosthesis
Phase Variable [22]	Level Walk, Stairs	2	2.3	Unilateral
A-ω [25]	Level Walk, Ramps, Run	2	1.9	Unilateral
A-ω [25]	Level Walk, Stairs, Jog	2	6.7	Unilateral
fuzzy-Logic [40]	level Walk, Stairs	3	0.6	Bilateral
DBN [39]	Level Walk, Stairs, Ramps	50	HS: 0.43, TO: 0.13	Prosthesis
IFI [41]	Level Walk, Stairs, Sit, Stand, Jog	86	2.32	Bilateral

* Dimension of feature space used to classify each activity type.
# Walk includes stand, level walking, ramp walking, and turning.
AB: able-bodied, AP: amputees
SS: steady-state, TS: transition
**: Bilateral: instrument both legs, Unilateral: instrument either leg.

existing activity recognition systems in terms of their classification methods, feature dimension, overall subject-independent error rate, and leg instrumentation. The overall accuracy of the presented system outperforms the other low-dimensional methods ($\leq$5 dimensions) with our simple 1-D feature space based on the ICFs. Similarities between level walking and ramps may introduce a higher error rate when these activities are separately classified [7], [13], [16], [21]. Although some papers reported higher accuracy [10], [39], those methods involved much higher-dimensional feature spaces by fusing multiple sensors. The kinematics-based SVM classification system [10] requires instrumentation of 7 IMUs on both legs, which involves a more intrusive experience than the presented method. The DBN classifier [39] can perform classifications with sensors onboard the prosthetic leg but requires a 90 ms delay to achieve the desired accuracy. The main distinction is that our ICFs are biomechanically and visually intuitive, so the presented system has the potential to be predictable to users so they can adapt to the classification rules over time [3].

E. Implications and Limitations

State-of-the-art wearable robots, including exoskeletons and prosthetic legs, typically have three levels of control [3]. The high-level controller determines the user's activity state/intent to pass onto the mid-level controller. Upon receiving the state, the mid-level controller maps sensor feedback (e.g., related to a phase variable) to the device's desired kinematic output and/or impedance for that activity state. The low-level controller closes the loop by feeding back the error between desired and actual trajectories to determine the joint torque (i.e., motor current). The presented classification system can serve as the high-level controller and integrate seamlessly with phase-variable based mid-level controllers [24], [26]–[29]. This combination would allow powered knee-ankle prostheses

to seamlessly transition between Sit, Walk, Stair Ascent, and Stair Descent while continuously adapting kinematics to estimates of so-called *task variables*, namely ground inclination and walking speed [28]. In this scenario, a single thigh-based IMU with foot contact information would be used for phase detection, transition detection, and task variable estimation.

If the mid-level controller needed to classify between level and ramp walking, it is possible to extend the presented method with certain modifications. During the offline training, the ramp data can be separated from the 'Walk' class to train the boundaries of ICFs, which will also add states to the current FSM. The corresponding ICFs of the ramps are in between the level walking and stair cases, which might lower the overall recognition accuracy (more misclassifications between these modes). Note that misclassifications between ramp descent and level walking can impact gait stability [4].

This study has several limitations in the experiment design and setup. First, the number of subjects in our offline analysis ($N = 10$) may not be enough to evaluate the subject dependency of our classification system, although similar sample sizes were used in previous studies [5], [7]–[16]. Second, although this system is ultimately intended for prosthetic leg users, we tested it with able-bodied subjects whose biological limbs will correctly transition regardless of the decision and timing of the classifier. We selected thigh-based ICFs specifically because above-knee amputees can control them through their intact hip, especially during the swing phase, as indicated in Section IV-C. Third, the subjects' training only lasted 10 minutes and did not allow long-term acclimation to the classification strategy, which caused some unnatural motion due to overthinking the classification rules. We observed continuous improvement during later trials of the post-training experiment, which suggests that extending the training period to approximately 30 minutes might encourage natural and consistent gait kinematics for detecting the ICFs.

V. Conclusion

We presented three thigh-based ICFs for an activity recognition system to classify transitions between activities in real-time. We evaluated the performance of the classification system using both offline and real-time experiments and found that our real-time system achieved an overall accuracy of 99.43%, pre-subject-training accuracy of 99.41%, and post-subject-training accuracy of 99.44% with less than 5 ms of classification latency. We believe this is a significant step towards clinically viable activity recognition systems for wearable robots. In future implementations on prosthetic legs, we will revisit the assumption of leading with the prosthetic side and perform real-time experiments with unilateral amputee subjects to make the system more robust for clinical purposes.

References

[1] P. T. Chinmilli, S. Redkar, W. Zhang, and T. Sugar, "A review on wearable inertial tracking based human gait analysis and control strategies of lower-limb exoskeletons," *Int. Robot. Autom. J.*, vol. 3, no. 7, pp. 398–415, Dec. 2017.

[2] S. J. Preece, J. Y. Goulermas, L. P. J. Kenney, D. Howard, K. Meijer, and R. Crompton, "Activity identification using body-mounted sensors—A review of classification techniques," *Physiological Meas.*, vol. 30, no. 4, pp. R1–R33, Apr. 2009.

[3] M. R. Tucker *et al.*, "Control strategies for active lower extremity prosthetics and orthotics: A review," *J. Neuroeng. Rehabil.*, vol. 12, no. 1, pp. 1–29, Dec. 2015.

[4] F. Zhang, M. Liu, and H. Huang, "Effects of locomotion mode recognition errors on volitional control of powered above-knee prostheses," *IEEE Trans. Neural Syst. Rehabil. Eng.*, vol. 23, no. 1, pp. 64–72, Jan. 2015.

[5] A. M. Boudali, P. J. Sinclair, and I. R. Manchester, "Predicting transitioning walking gaits: Hip and knee joint trajectories from the motion of walking canes," *IEEE Trans. Neural Syst. Rehabil. Eng.*, vol. 27, no. 9, pp. 1791–1800, Sep. 2019.

[6] K. Zhang *et al.*, "A subvision system for enhancing the environmental adaptability of the powered transfemoral prosthesis," *IEEE Trans. Cybern.*, vol. 51, no. 6, pp. 3285–3297, Jun. 2021.

[7] A. J. Young and L. J. Hargrove, "A classification method for user-independent intent recognition for transfemoral amputees using powered lower limb prostheses," *IEEE Trans. Neural Syst. Rehabil. Eng.*, vol. 24, no. 2, pp. 217–225, Feb. 2016.

[8] S. M. R. Sorkhabadi, P. T. Chinimilli, D. Gaytan-Jenkins, and W. Zhang, "Human locomotion activity and speed recognition using electromyography based features," in *Proc. Wearable Robot. Assoc. Conf. (WearRAcon)*, Mar. 2019, pp. 80–85.

[9] A. J. Young, A. M. Simon, N. P. Fey, and L. J. Hargrove, "Intent recognition in a powered lower limb prosthesis using time history information," *Ann. Biomed. Eng.*, vol. 42, no. 3, pp. 631–641, Mar. 2014.

[10] J. Figueiredo, S. P. Carvalho, D. Goncalve, J. C. Moreno, and C. P. Santos, "Daily locomotion recognition and prediction: A kinematic data-based machine learning approach," *IEEE Access*, vol. 8, pp. 33250–33262, 2020.

[11] H. Huang, F. Zhang, L. J. Hargrove, Z. Dou, D. R. Rogers, and K. B. Englehart, "Continuous locomotion-mode identification for prosthetic legs based on neuromuscular-mechanical fusion," *IEEE Trans. Biomed. Eng.*, vol. 58, no. 10, pp. 2867–2875, Oct. 2011.

[12] M. Zeng *et al.*, "Convolutional neural networks for human activity recognition using mobile sensors," in *Proc. 6th Int. Conf. Mobile Comput., Appl. Services*, 2014, pp. 197–205.

[13] U. H. Lee, J. Bi, R. Patel, D. Fouhey, and E. Rouse, "Image transformation and CNNs: A strategy for encoding human locomotor intent for autonomous wearable robots," *IEEE Robot. Autom. Lett.*, vol. 5, no. 4, pp. 5440–5447, Oct. 2020.

[14] D. Ravi, C. Wong, B. Lo, and G.-Z. Yang, "Deep learning for human activity recognition: A resource efficient implementation on low-power devices," in *Proc. IEEE 13th Int. Conf. Wearable Implant. Body Sensor Netw. (BSN)*, Jun. 2016, pp. 71–76.

[15] B.-Y. Su, J. Wang, S.-Q. Liu, M. Sheng, J. Jiang, and K. Xiang, "A CNN-based method for intent recognition using inertial measurement units and intelligent lower limb prosthesis," *IEEE Trans. Neural Syst. Rehabil. Eng.*, vol. 27, no. 5, pp. 1032–1042, May 2019.

[16] K. Bhakta, J. Camargo, L. Donovan, K. Herrin, and A. Young, "Machine learning model comparisons of user independent & dependent intent recognition systems for powered prostheses," *IEEE Robot. Autom. Lett.*, vol. 5, no. 4, pp. 5393–5400, Oct. 2020.

[17] H. A. Varol, F. Sup, and M. Goldfarb, "Multiclass real-time intent recognition of a powered lower limb prosthesis," *IEEE Trans. Biomed. Eng.*, vol. 57, no. 3, pp. 542–551, Mar. 2010.

[18] C. E. Roffman, J. Buchanan, and G. T. Allison, "Predictors of non-use of prostheses by people with lower limb amputation after discharge from rehabilitation: Development and validation of clinical prediction rules," *J. Physiotherapy*, vol. 60, no. 4, pp. 224–231, Dec. 2014.

[19] S. Culver, H. Bartlett, A. Shultz, and M. Goldfarb, "A stair ascent and descent controller for a powered ankle prosthesis," *IEEE Trans. Neural Syst. Rehabil. Eng.*, vol. 26, no. 5, pp. 993–1002, May 2018.

[20] R. Stolyarov, M. Carney, and H. Herr, "Accurate heuristic terrain prediction in powered lower-limb prostheses using onboard sensors," *IEEE Trans. Biomed. Eng.*, vol. 68, no. 2, pp. 384–392, Feb. 2021.

[21] F. Gao, G. Liu, F. Liang, and W.-H. Liao, "IMU-based locomotion mode identification for transtibial prostheses, orthoses, and exoskeletons," *IEEE Trans. Neural Syst. Rehabil. Eng.*, vol. 28, no. 6, pp. 1334–1343, Jun. 2020.

[22] H. L. Bartlett and M. Goldfarb, "A phase variable approach for IMU-based locomotion activity recognition," *IEEE Trans. Biomed. Eng.*, vol. 65, no. 6, pp. 1330–1338, Jun. 2018.

[23] M. A. Holgate, T. G. Sugar, and A. W. Bohler, "A novel control algorithm for wearable robotics using phase plane invariants," in *Proc. IEEE Int. Conf. Robot. Autom.*, May 2009, pp. 3845–3850.

[24] D. Quintero, D. J. Villarreal, D. J. Lambert, S. Kapp, and R. D. Gregg, "Continuous-phase control of a powered knee–ankle prosthesis: Amputee experiments across speeds and inclines," *IEEE Trans. Robot.*, vol. 34, no. 3, pp. 686–701, Jun. 2018.

[25] P. T. Chinimilli, S. Redkar, and T. Sugar, "A two-dimensional feature space-based approach for human locomotion recognition," *IEEE Sensors J.*, vol. 19, no. 11, pp. 4271–4282, Jun. 2019.

[26] S. Rezazadeh, D. Quintero, N. Divekar, E. Reznick, L. Gray, and R. D. Gregg, "A phase variable approach for improved rhythmic and non-rhythmic control of a powered knee–ankle prosthesis," *IEEE Access*, vol. 7, pp. 109840–109855, 2019.

[27] T. Elery, S. Rezazadeh, E. Reznick, L. Gray, and R. D. Gregg, "Effects of a powered knee–ankle prosthesis on amputee hip compensations: A case series," *IEEE Trans. Neural Syst. Rehabil. Eng.*, vol. 28, no. 12, pp. 2944–2954, Dec. 2020.

[28] K. R. Embry and R. D. Gregg, "Analysis of continuously varying kinematics for prosthetic leg control applications," *IEEE Trans. Neural Syst. Rehabil. Eng.*, vol. 29, pp. 262–272, 2021.

[29] D. Raz, E. Bolívar-Nieto, N. Ozay, and R. D. Gregg, "Modeling and phase-variable control of sit-to-stand motion with a powered knee-ankle prosthesis," in *Proc. IEEE Conf. Control Technol. Appl.*, Jan. 2021, pp. 1–7.

[30] E. Reznick, K. Embry, R. Neuman, E. Bolívar-Nieto, N. P. Fey, and R. D. Gregg, "Lower-limb kinematics and kinetics during continuously varying human locomotion," 2021, *arXiv:2108.12307*. [Online]. Available: https://arxiv.org/abs/2108.12307

[31] A. Azocar, L. Mooney, J. Duval, A. Simon, L. Hargrove, and E. Rouse, "Design and clinical implementation of an open-source bionic leg," *Nature Biomed. Eng.*, vol. 4, no. 10, pp. 941–953, 2020.

[32] M. K. Ishmael, M. Tran, and T. Lenzi, "ExoProsthetics: Assisting above-knee amputees with a lightweight powered hip exoskeleton," in *Proc. IEEE 16th Int. Conf. Rehabil. Robot. (ICORR)*, Jun. 2019, pp. 925–930.

[33] E. Fullerton, B. Heller, and M. Munoz-Organero, "Recognizing human activity in free-living using multiple body-worn accelerometers," *IEEE Sensors J.*, vol. 17, no. 16, pp. 5290–5297, Aug. 2017.

[34] N. Abhayasinghe, I. Murray, and S. S. Bidabadi, "Validation of thigh angle estimation using inertial measurement unit data against optical motion capture systems," *Sensors*, vol. 19, no. 3, p. 596, Jan. 2019.

[35] LORD MicroStrain. *3DM-GX5-25 Attitude and Heading Reference System (AHRS)*. Accessed: Aug. 26, 2021. [Online]. Available: https://www.microstrain.com/sites/default/files/3dm-gx5-25_datasheet_8400-0093.pdf

[36] J. Camargo, A. Ramanathan, W. Flanagan, and A. Young, "A comprehensive, open-source dataset of lower limb biomechanics in multiple conditions of stairs, ramps, and level-ground ambulation and transitions," *J. Biomechanics*, vol. 119, Apr. 2021, Art. no. 110320.

[37] F. Zhang, M. Liu, and H. Huang, "Investigation of timing to switch control mode in powered knee prostheses during task transitions," *PLoS ONE*, vol. 10, no. 7, Jul. 2015, Art. no. e0133965.

[38] *2010 ADA Standards for Accessible Design*, Dept. Justice, Washington, DC, USA, 2010.

[39] A. M. Simon *et al.*, "Delaying ambulation mode transition decisions improves accuracy of a flexible control system for powered knee-ankle prosthesis," *IEEE Trans. Neural Syst. Rehabil. Eng.*, vol. 25, no. 8, pp. 1164–1171, Aug. 2017.

[40] A. Parri *et al.*, "Real-time hybrid locomotion mode recognition for lower limb wearable robots," *IEEE/ASME Trans. Mechatronics*, vol. 22, no. 6, pp. 2480–2491, Dec. 2017.

[41] P. T. Chinimilli, S. Redkar, and W. Zhang, "Human activity recognition using inertial measurement units and smart shoes," in *Proc. Amer. Control Conf. (ACC)*, May 2017, pp. 1462–1467.